Investigation of Cracks Found in Helicopter Longerons

John A. Newman[1*], James M. Baughman[2], and Terryl A. Wallace[1]

[1] NASA Langley Research Center, MS 188E, Hampton, VA 23681
[2] Lockheed Martin Space Operations, Langley Research Center, MS 188E, Hampton, VA 23681

Abstract: Four cracked longerons, containing a total of eight cracks, were provided for study. Cracked regions were cut from the longerons. Load was applied to open the cracks, enabling crack surface examination. Examination revealed that crack propagation was driven by fatigue loading in all eight cases. Fatigue crack initiation appears to have occurred on the top edge of the longerons near geometric changes that affect component bending stiffness. Additionally, metallurigical analysis has revealed a local depletion in alloying elements in the crack initiation regions that may be a contributing factor. Fatigue crack propagation appeared to be initially driven by opening-mode loading, but at a crack length of approximately 0.5 inches (12.7 mm), there is evidence of mixed-mode crack loading. For the longest cracks studied, shear-mode displacements destroyed crack-surface features of interest over significant portions of the crack surfaces.

Keywords: Crack, Fatigue, Aluminum alloy 7075, Fatigue striation, Helicopter.

1. Introduction

An investigation was performed to determine the root cause of cracks found in longerons located in the tail-boom fairing of MD 500 series helicopters. The tail-boom fairing section has a conical shape that is normally oriented horizontally, as shown in Figure 1a. A schematic of the tail-boom cross section is shown in Figure 1b where the aircraft skin and longerons are labeled. For this configuration, the longerons are oriented horizontally, one each on the starboard and port sides of the vehicle. All longerons provided for study were removed from the starboard side of the helicopter. The longerons are constructed from 0.025-inch-thick (0.635 mm) 7075 aluminum sheet that is stamped into its final shape shown in Figure 2a. These longerons are approximately 48 inches (1.22 m) long and are connected to both the tail-boom fairing skin (0.016-inch-thick (0.41 mm) aluminum sheet material) and a series of structural bulkheads (0.025-inch-thick (0.635 mm) aluminum sheet material). Each longeron consists of a series of

sections that are bent into a "J" shape for increased bending stiffness, as shown in Figure 2b. Between the stiffened sections, the longeron remains a flat 0.025-inch-thick (0.635 mm) sheet, approximately 2 inches (50.8 mm) wide, as shown in Figure 2c, to allow the longeron to pass between a bulkhead and the skin (Stations 146.62, 155.75, 164.87, and 174.00, as indicated in Figure 2).[†] Each end of a longeron terminates under a bulkhead with a flat low-bending-stiffness region (Stations 137.50 and 185.89, as indicated in Figure 2).

For these longerons, the orientations of Figures 1 and 2 are consistent in that the left direction in these figures corresponds to the forward direction on the vehicle. A total of eight (8) cracks were found in the four (4) longerons provided, as summarized in Table 1. All cracks were located in the low stiffness (flat) regions, in close proximity to the stiffened section. A typical crack is shown in Figure 3a. For this crack (Longeron #2, Crack #2), some secondary cracking was observed at a nearby fastener hole. With respect to the longeron orientation of Figure 2, every crack occurred on the left (forward) side of the bulkhead attachment station and appeared to initiate from the top edge region of the longeron. Some of the longeron cracks were observed to have some residual shear displacement such that the crack faces appeared as in Figure 3b, while other cracks did not exhibit this residual shear displacement and appeared similar to that shown in Figure 3c. The cracks with notable residual shear displacements (Longeron #1, Crack #1; Longeron #2, Crack #1; and Longeron #4, Crack #1) were the longest cracks examined (approximately greater than 0.5 inches (12.7 mm)). These observations suggest that cracks initially grew without obvious shear deformations and that this deformation mode became more significant as the crack length increased.

The cracked regions were cut away leaving a small uncracked ligament (typically 1/16 to 1/8 inch (1.59 mm to 3.18 mm)) that was easily fractured open exposing the cracks surfaces for analysis. As appropriate, crack surfaces were ultrasonically cleaned in acetone to remove debris. An Energy Dispersive X-ray (EDX) analysis of the crack surface debris was performed to characterize the chemistry prior to crack surface cleaning. Crack surface features were examined using both an optical microscope and a scanning electron microscope (SEM). Additionally, the chemistry (EDX) and microstructure (using Electron Back-Scatter Diffraction, EBSD) of the longeron sheet material were characterized in the apparent regions of crack initiation.

* Corresponding author; Email: john.a.newman@nasa.gov; Tel: 757-864-8945; FAX: 757-864-8911
† Station numbers correspond to the distance from the front of the aircraft, in inches.

The objective of this study was to characterize the failure surfaces to determine the root cause of cracking. These results, along with stress analysis results provided by the manufacturer, will be used to develop a solution to this cracking problem.

2. Observations

In this report, results are presented for each of the eight cracks. SEM images for each of the crack surfaces are presented in the following sections, and crack surface features provide evidence that in all cases examined, crack growth was driven by fatigue (cyclic) loading.

2.1 Longeron #1, Crack #1

SEM crack-surface micrographs for Longeron #1, Crack #1 (a crack approximately 0.85 inches long (21.59 mm) that initiated at Station 164.87) are shown in Figure 4. In Figure 4a, the sheet thickness direction is oriented vertically with the top edge of the longeron on the left side of the figure. Bright white regions seen on the outer surfaces of the sheet are paint. Large portions of the crack surface appear to be damaged or smeared, likely a result of the crack surfaces coming into contact with each other. Crack-surface features that may have been in these damaged regions have been destroyed; however, there are undamaged regions of the crack surface where striations have been found, and are shown at higher magnification in Figures 4b and 4c. These striations are compelling evidence that crack growth was driven by fatigue loading (ref. 1). Additionally, river marks (fatigue crack surface features that are typically perpendicular to striations, oriented parallel to the direction of crack growth) are labeled in Figure 4b.

2.2 Longeron #1, Crack #2

Crack-surface examinations of Longeron #1, Crack #2 (a crack approximately 0.38 inches long (9.65 mm) occurring at Station 155.75), reveals the presence of fatigue striations, microscopic features consistent with fatigue crack growth (see Figure 5). A lower-magnification image of the crack surface is shown in Figure 5a corresponding to the top side of the longeron in the region where crack initiation appears to occur. The sheet thickness (0.025-inch-thick) direction is oriented vertically in this image. Two regions of interest are denoted, which are shown at higher-magnification in Figures 5b and 5c. Fatigue striations are easily identified in Figure 5b and at multiple other locations on the crack surface (ref. 1). The slight curvature of these striations (indications of the crack front at some previous point in time) can be traced back to determine the crack initiation site, which is shown at higher-magnification in

Figure 5c. Crack-surface features suggest that the location of crack initiation was near the surface of the sheet material. No obvious defect in the region of crack initiation was noted (e.g., corrosion pit, scratch, tool mark, etc.). The bright region near the outer surface of the sheet (extreme right side of Figure 5c) is a result of the paint covering the longeron.

2.3 Longeron #1, Crack #3

SEM crack-surface micrographs for Longeron #1, Crack #3 (a crack approximately 0.15 inches long (3.81 mm) that initiated at Station 185.89) are shown in Figure 6. The crack surface corresponding to the top edge of the longeron is shown in Figure 6a, where the top edge of the longeron is on the left side of the figure and the sheet thickness direction is vertical. Paint on the surface of the longeron is seen as the bright white regions near the top and bottom of the figure. The crack surface is nearly free of mechanical contact damage and striations can be readily observed over nearly the entire surface (ref. 1). A typical striated region is shown in Figure 6b. Striations can be traced back to an apparent origin, which is located near the top left corner of the sheet, with respect to the orientation presented in Figure 6a, and is shown at higher magnification in Figure 6c.

2.4 Longeron #2, Crack #1

SEM crack-surface micrographs for Longeron #2, Crack #1 (a crack approximately 0.62 inches long (15.75 mm) that initiated at Station 146.62) are shown in Figure 7. A lower-magnification image of the crack surface corresponding to the top edge of the longeron (apparent crack initiation region) is shown in Figure 7a. A higher-magnification image of the crack surface, corresponding to the upper left corner of Figure 7a, is shown in Figure 7b. Here, the crack surface appears to be smeared (contact damage) such that most of the crack-surface features (e.g., fatigue striations) have been destroyed. However, further from the top edge of the longeron (crack surface regions corresponding to the left side of Figure 7a), fatigue striations are observed (ref. 1). A typical region of fatigue striations is shown at high magnification in Figure 7c.

2.5 Longeron #2, Crack #2

SEM crack-surface micrographs for Longeron #2, Crack #2 (a crack approximately 0.44 inches long (11.18 mm) that initiated at Station 164.87) are shown in Figure 8. The crack surface near the top edge of the longeron is shown at lower-magnification in Figure 8a. A higher-magnification image of the crack surface, corresponding to the upper left corner of Figure 8a, is shown as Figure 8b. Similar to the results previously shown in Figure 7 (Longeron #2, Crack #1), the crack surface appears to be smeared (contact

damage) such that most of the crack-surface features, like fatigue striations (if they did exist), have been destroyed. However, there are a few islands of undamaged crack surface that contain striations (ref. 1). An example of these striations is shown in Figure 8c. Here, "river marks" (fatigue crack surface features that are typically perpendicular to striations, oriented parallel to the direction of crack growth) can be seen oriented vertically and striations are seen arcing across the image, as the crack appeared to grow from the upper left corner of the figure to the lower right. In this image, a third set of interesting linear features can be seen that are believed to be grain boundaries (ref. 1). Here, it is believed that the region containing the clear striations is within a grain oriented in a manner to promote striations while the regions above and below are grains having different orientations such that striations are less pronounced. If these features are indeed grain boundaries, the grains in this sheet product are elongated in the sheet directions and thin in the direction of the sheet thickness. Further work is needed to characterize the microstructure of this sheet product.

2.6 Longeron #3, Crack #1

SEM crack-surface micrographs for Longeron #3, Crack #1 (a crack approximately 0.31 inches long (7.87 mm) that initiated at Station 164.87) are shown in Figure 9. The crack surface region near the top edge of the longeron is shown at lower-magnification in Figure 9a. A higher-magnification image of the surface near the edge is shown in Figure 9b. Here, the top edge of the longeron sheet is on the left side of Figure 9b; the bright area corresponds to the paint on the outer surface. Similar to the results for the cracks found in Longeron #2, portions of the crack surface appear to be smeared or damaged. However, islands of undamaged surface can be seen near the center of Figure 9b. Some of these undamaged regions are striated, as shown in Figure 9c, indicating that the crack propagation was driven by cyclic loading (ref. 1).

2.7 Longeron #4, Crack #1

SEM crack-surface micrographs for Longeron #4, Crack #1 (a crack approximately 0.49 inches long (12.45 mm) that initiated at Station 155.75) are shown in Figure 10. A relatively low-magnification image of the entire sheet thickness is shown as Figure 10a; here, the top edge of the longeron corresponds to the left side of the figure. Large portions of the crack surface appear to be damaged, presumably smeared as crack faces came into sliding contact, as observed in Figure 3b. In these damaged regions, crack-surface features of interest have been destroyed. A higher-magnification image of the damaged corner region is shown as Figure 10b. However, there are crack-surface regions that escaped mechanical

damage and in these regions fatigue striations were observed (ref. 1). A typical example of striations in these undamaged regions is shown as Figure 10c.

2.8 Longeron #4, Crack #2

SEM crack-surface micrographs for Longeron #4, Crack #2 (a crack approximately 0.18 inches long (4.57 mm) that initiated at Station 164.87) are shown in Figure 11. A relatively low-magnification image of the entire sheet thickness is shown as Figure 11a; here, the top edge of the longeron corresponds to the right side of the figure. Recall from Figure 3b that this relatively short crack exhibited no residual shear displacement. It is likely not coincidental that these crack surfaces are nearly free of contact or smearing damage. Nearly the entire crack surface contains fatigue striations (ref. 1). These fatigue striations can be traced back to an apparent crack initiation site, which is shown at higher magnification as Figure 11b. No obvious crack initiation feature (e.g., scratch, pit, or other defect) was observed near the crack initiation site, which suggests that surface defects were not a contributing factor in crack initiation. Fatigue striations are shown at high magnification in Figure 11c. In this image, the crack surface appears similar to that of Longeron #2, Crack #2 (Figure 8c) and Longeron #3, Crack #1 (Figure 9c), where features that are believed to be grain boundaries can be identified in the image.

2.9 EDX Examination of Crack-Surface Debris

Typically, the crack surfaces were covered with debris that obscured the microscopic features of interest. To examine these features, the crack surfaces were ultrasonically cleaned in acetone, which successfully removed most of the debris without damaging the crack surfaces or the paint on the external surfaces of the longerons. The SEM images shown in Figures 4-11 were taken from clean surfaces. However, before cleaning, the dirty surfaces were examined in the SEM and chemically analyzed using Energy Dispersive X-ray (EDX) Spectroscopy (ref. 2). Crack surfaces of Longeron #3, Crack #1 are shown in Figure 12 both before cleaning the crack surfaces (Figure 12a) and after cleaning (Figure 12b). The crack surface debris is readily seen as the bright white regions in Figure 12a (absent in Figure 12b), a result of surface charging in the electron beam of the SEM. An EDX analysis taken of the debris (white regions in Figure 12a) indicates the presence of chlorine (25.3% weight), oxygen (16.6%), silicon (15.7%), sulfur (11.3%), sodium (9.0%), potassium (7.4%), phosphorus (6.0%), calcium (5.4%), and aluminum (3.3%). Similar chemical signatures have been obtained from other crack surfaces.

3. Metallurgical Analysis

The crack surfaces shown as Figures 8c, 9c, and 11c revealed a series of interesting linear features. Striations (perpendicular to the direction of crack growth) and river marks (parallel to the direction of crack growth) are compelling evidence of fatigue crack growth (crack growth driven by cyclic loading; ref. 1). Another series of parallel linear features (spaced approximately 20 μm apart) observed were believed to be grain boundaries, suggesting that the aluminum sheet microstructure may affect fatigue crack growth. Thus, the grain structure of the longeron sheet material was characterized to confirm that the features of interest in Figures 8c, 9c, and 11c are indeed grain boundaries, approximately 20 μm thick in the sheet thickness direction.

The microstructure of the aluminum alloy 7075 sheet is shown in Figure 13. For this microstructual analysis, a sample of material was cut from Longeron #1, immediately aft of Station 155.75. As indicated by the boxed region in Figure 13a, the material analyzed corresponded to the portion of the longeron that was fastened to the tail-boom fairing skin. Surfaces normal to the sheet directions were cut, mounted, etched[‡] and polished for metallurgical analysis, and the corresponding images were arranged to appear as a three-dimensional cube of the material, herein termed "orthogonal metallurgical cube." See Figure 13b for an orthogonal metallurgical cube of the longeron sheet material; here, the bottom edge of Figure 13b corresponds to the outer edge of the longeron sheet. The orthogonal surfaces used were termed "L" (perpendicular to the length of the longeron), "T" (perpendicular to the vertical longeron direction as described in Figure 1), and "S" (perpendicular to the 0.025-inch sheet thickness direction). Examination of the dark lines in Figure 13b (presumably grain boundaries) indicates large grain areas on the S-surface with long and flat grain areas along both the L-surfaces and T-surfaces. These observations are typical of aluminum sheet material and a flattened pancake-shape grain structure. A portion of Figure 13b is shown at higher magnification in Figure 13c to better show microstructural boundaries. Here, the typical spacing between linear indications on both the L-surfaces and T-surfaces is nearly 20 μm, consistent with the hypothesis that the features observed in Figures 8c and 9c are grain boundaries

To confirm that the linear indications observed in Figure 13 are indeed grain boundaries, the physical metallurgy of the sheet material was analyzed using an SEM equipped with Electron Back-Scatter Diffraction (EBSD) to generate crystal orientation maps (ref. 2). A section of the longeron material (cut from Longeron #1, immediately aft of Station 155.75) was mounted and prepared for EBSD analysis, exposing a surface normal to the L-direction as defined in Figure 13, and having the same nominal

orientation as the crack faces. The sample was mounted in an epoxy material to preserve the integrity of the edges (prevent rounding during polishing) and polishing was performed with care to eliminate surface residual stresses. EBSD data were collected across the sample, and then analyzed to produce crystal orientation maps of the near-sheet-surface material, which are presented in Figure 14. Figure 14b is a higher-magnification crystal orientation map of region B, which is indicated in Figure 14a. The paint, near surface area, and interior regions are indicated in Figure 14b. The crystal orientation map consists of thousands of points, each assigned a color based on its crystal orientation. In this image, grains appear as continuous regions having the same color. The grains seen in the interior region appear to be elongated and approximately 25 μm thick (in the sheet thickness direction, seen in Figure 14 as the vertical direction), which is consistent with the grain size estimates obtained from SEM observations of Figures 8c, 9c, and 11c. The grains within 25 μm of the sheet surface have a significantly smaller grain size compared with the interior region.

Examination of the orthogonal metallurgical cube of Figure 13b reveals the presence of what appears to be a dark band near the outer surface of the sheet material (see bottom of Figure 13b). This discoloration occurred in the same near-surface region where small grain sizes were observed (recall Figure 14). A chemical analysis (EDX) was performed on near-surface and interior regions of the polished surfaces. SEM images of regions examined are shown in Figure 15. In these images, the sheet material is seen at the bottom with the paint layer near the top. The near surface region selected for analysis is shown with a box in Figure 15a and the interior region (approximately 60 μm from the surface) is indicated by a box in Figure 15b. The chemical analysis results, which are summarized in Table 2, indicate that the near surface region contains less alloying elements (zinc, copper, and magnesium) than the interior region, which has a composition typical of aluminum alloy 7075 (ref. 4). This depletion of alloying elements at the surface may result in a degradation of mechanical properties, such as poor resistance to crack initiation. In all cases where crack surface observations permitted (recall Figures 5, 6, and 11), crack initiation sites were always located on the corner of the longeron cross-section near the intersection of sheet surface (where a depletion of alloying elements was observed) and the top edge of the longeron where bending stresses are likely greatest. Further study is needed to determine if the chemical depletion contributed to the cracking.

---

‡ Polished surfaces were etched to highlight grain boundaries and other microstructural features. Keller's etchant was used with surfaces exposed for approximately 30 seconds (ref. 3).

4. Discussion

Four longerons were provided for study, containing a total of eight cracks, ranging in crack size from 0.85 inches to 0.015 inches long. The most obvious and consistent observation is that all crack surfaces contained compelling evidence that crack growth was driven by fatigue loading (e.g., striations) (ref. 1). In some cases, portions of the crack surfaces were damaged, locally destroying crack surface features of interest. In this section, a few additional observations are made.

4.1 Correlation of Increasing Crack Length, Crack-surface Damage, and Shear Displacements

Several of the crack surfaces examined appeared to contain regions of mechanical damage where crack surface features were obliterated, presumably by crack surfaces coming into contact with each other (Longeron #1, Crack #1; Longeron #2, Crack #1,; Longeron #2, Crack #2; Longeron #4, Crack#1). These were the longest cracks examined and were the same cracks that exhibited residual shear displacements. (Recall, an example of residual shear deformation was shown in Figure 3b.) It seems highly likely that the surface damage observed was a result of crack surface contact from shear (or mode III) displacements. Without knowledge of the load transfer within the structure, it is difficult to determine if the crack propagated under mixed-mode loading from the onset of crack growth, or if the crack growth caused local load redistribution and produced mixed-mode crack-tip loading only as the crack grew to a significant length (perhaps something like 0.5 inches (12.7 mm)). The most severe damage was observed on the crack surfaces nearest the top edge of the longeron, corresponding to the likely location of crack initiation. During the later stages of crack propagation, this region is the furthest from the crack-tip where crack opening and sliding displacements are expected to be largest, which is more damaging in terms of mechanical crack-face contact damage.

Finally, it is possible that residual shear displacements were not a product of service loading, but were imparted on the structure during component removal. The two smallest cracks (Longeron #1, Crack #3 and Longeron #4, Crack #2) were only discovered during examination at NASA (not found during Army inspections), and these cracks were considered to be "tight," meaning that these cracks appeared as a fine linear indication without obvious residual shear deformation. Therefore, it seems likely that the visual inspection performed as routine maintenance, was only able to detect highly-visible cracks with significant shear displacements. Specifically, cracks with significant residual shear displacements expose a portion of the crack face, providing visual contrast with the painted (green) longeron surface, enhancing crack detection.

4.2 Metallurgical Analysis

During metallurgical analysis of the longeron sheet material, an unusual feature was observed on polished surfaces of near-surface samples. (Recall, this layer appeared as a dark band near the bottom of Figure 13b.) Chemical analysis of near-surface region (Figure 14a) revealed that, in comparison to both the interior chemistry and typical aluminum alloy 7075 chemistry (ref. 4), it was relatively poor in the alloying elements copper, zinc, and magnesium, and appeared to contain traces of iron. This alloying element depletion may result in a local degradation in mechanical performance, including resistance to cracking. In the examples where crack-surface features were used to determine an apparent crack initiation site (Longeron #1, Crack #2; Longeron #1, Crack #3), these crack initiation sites occurred near the longeron sheet surface (where alloying element depletion was observed). EBSD results (Figure 15) revealed that the typical grain sizes within this near-surface alloying-element-depletion region were significantly finer than those within the longeron sheet interior. Additionally, the absence of corrosion pits, scratches, dents, or tool marks, suggests that corrosion and handling (e.g., installation and maintenance) were not contributing factors on crack initiation.

Crack-surface debris originally obstructed portions of the crack surface, especially the portions of the crack surface where crack initiation is presumed to have occurred. Cleaning of the crack surface was necessary to observe crack surface features of interest. As a precautionary measure, crack-surface debris was chemically analyzed before removal in case this substance was later found to contribute to crack initiation or propagation. No evidence was found to suggest that the crack-surface debris influenced crack initiation or propagation.

4.3 Likely Progression-of-damage Scenario

The following findings are considered most significant in determining the progression-of-damage scenario. First, the observation that fatigue striations were found on nearly every crack surface region that did not appear to be damaged (likely a result of crack-face contact), and for all eight cracks, suggests that crack propagation was driven by fatigue (cyclic) loading (ref. 1). Second, there is some evidence for the longer cracks that shear-mode loading occurred, specifically, residual shear displacements (recall Figure 3b). However, for the smaller cracks, there is no obvious evidence of anything but opening mode (mode I) loading. Generally, cracks tend to orient themselves such that they propagate on planes perpendicular to the largest principal normal stress (ref. 5). However, complex flight profiles may produce significant variations in principal stress directions that are well beyond the scope of this study. The findings of this study suggest that cracks propagated under nominal mode I loading until reaching a

critical size, possibly on the order of 0.5 inches (12.7 mm) in length, but this may vary based on actual flight conditions. Third, near the surfaces of the longeron sheet material, a depletion of alloying elements was observed, possibly resulting in inferior mechanical performance (e.g., crack initiation).

Based on these findings, the most likely progression-of-damage scenario is that crack initiation occurred near the top edge of the longeron, where multiple factors made crack initiation likely including (1) high bending stress, (2) low bending stiffness, and (3) potential degradation in mechanical properties due to local depletion of alloying elements. It is not clear if crack initiation was chemically or environmentally assisted, but fatigue loading likely played a very significant role (if not the sole contributing factor), and crack propagation was definitely driven by fatigue loading. Cracks appeared to propagate under nominal opening mode (mode I) loading until reaching a crack length on the order of 0.5 inches. At this point, shear mode (mode III) loading is believed to have become significant, possibly due to local redistribution of loading, but not enough is known about the surrounding structure to develop supporting evidence, and such stress analysis is beyond the scope of this study. These shear mode displacements, reserved for the longest of the cracks, abraded the crack surfaces destroying crack surface features of interest over a portion of the crack surfaces. Sometime during the crack propagation phase, the debris accumulated on the crack faces. As the chemical composition differed from the composition of the aluminum alloy 7075 longeron sheet, the crack-surface debris must have come from an external source. No evidence exists to suggest that the crack-surface debris contributed to the initiation or propagation of cracks. Further, no obvious damage or breach in the protective paint coating the external surfaces of the longerons was observed at the locations of apparent crack initiation.

5. Summary

An effort was undertaken to investigate the cause of cracks found in four MD 500 helicopter tail-boom longerons. A total of eight cracks were identified and examined using microscopic analysis techniques. Compelling evidence was presented that conclusively showed that in all eight cases studied, crack propagation was driven by fatigue loading. Fatigue crack initiation is believed to have occurred at high-stress regions on the top edge of the longerons characterized by a transition in local bending stiffness. A local depletion in alloying elements may also result in a degradation of mechanical properties, affecting the crack growth behavior. The absence of corrosion pitting, scratches, or tool marks in the crack initiation regions suggest that corrosion or local defects were not a contributing factor. Fatigue crack propagation appeared to be initially driven by opening mode loading, but as the crack length approached 0.5 inches (12.7 mm) in length, there is evidence that mixed-mode crack loading occurred. For the

longest cracks studied, shear mode displacements destroyed crack-surface features of interest over a significant portion of the crack surfaces.

6. References

1. ASM Handbook, Volume 12, *Fractography*, ASM International, Materials Park, OH 2007.

2. J.I. Goldstein, D.E. Newbury, D.C. Joy, C.E. Lyman, P. Echlin, E. Lifshin, L. Sawyer, and J.R. Michael, *Scanning Electron Microscopy and X-ray Microanalysis, 3rd Edition*, Springer Science+Business Media, New York, NY, 2003, pp. 297-323.

3. Metallographic Etching, 2nd Edition, ASTM International, 1999, p. 188.

4. J.E. Hatch, Editor, *Aluminum: Properties and Physical Metallurgy*, American Society for Metals, Metals Park, OH, 1984, p. 354.

5. F. Erdogan and G.C. Sih, "On the Crack Extension in Plates Under Plane Loading and Transverse Shear," Journal of Basic Engineering, Dec. 1963, pp. 519-527.

Table 1. Summary of cracks found in longerons provided for analysis.

Longeron number	Year of manufacture	Crack number	Crack Location	Crack length, mm (inch)
1	2003	1	Station 164.87	21.59 (0.85)
		2	Station 155.75	9.65 (0.38)
		3	Station 185.89	3.81 (0.15)
2	1981	1	Station 146.62	15.75 (0.62)*
		2	Station 164.87	11.18 (0.44)
3	2006	1	Station 164.87	7.87 (0.31)
4	2001	1	Station 155.75	12.45 (0.49)
		2	Station 164.87	4.57 (0.18)

* Crack terminated at fastener hole

Table 2. Comparison of near-surface and interior alloy chemistry.

Element	Near-Surface (weight %)	Interior (weight %)	Nominal (ref.4) (weight %)
Aluminum, Al	93.71	89.69	88.90
Magnesium, Mg	1.25	2.26	2.40
Copper, Cu	0.53	1.80	2.20
Zinc, Zn	4.30	6.25	6.40
Iron, Fe	0.22	-	-

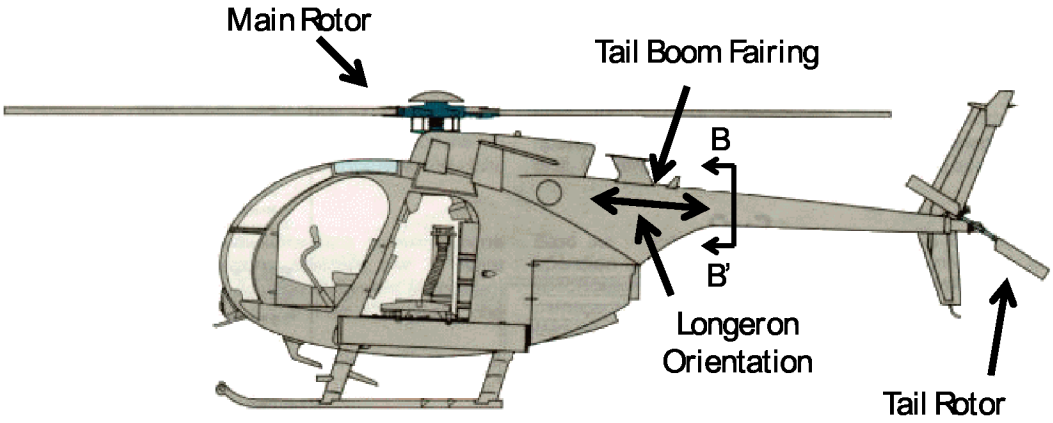

(a) Configuration of MD 500 helicopter.

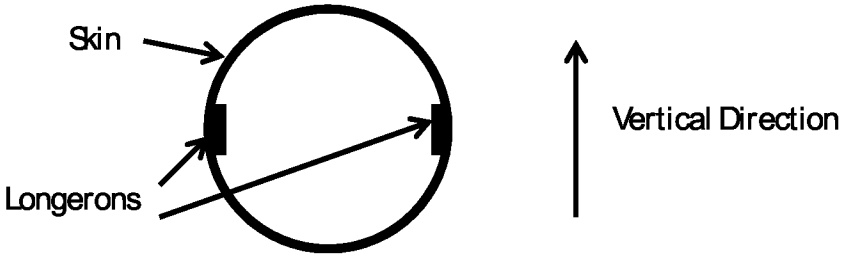

(b) Schematic of tail-boom cross section (B-B′).

Figure 1. Locations of longerons on the MD 500 helicopter.

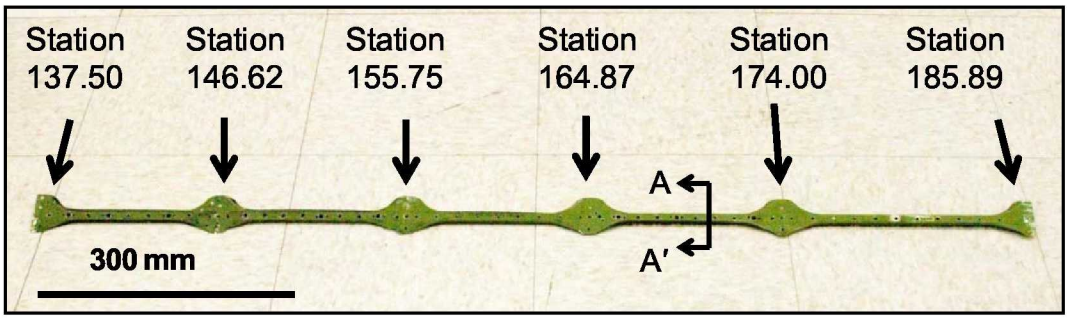

(a) Photograph of entire longeron.

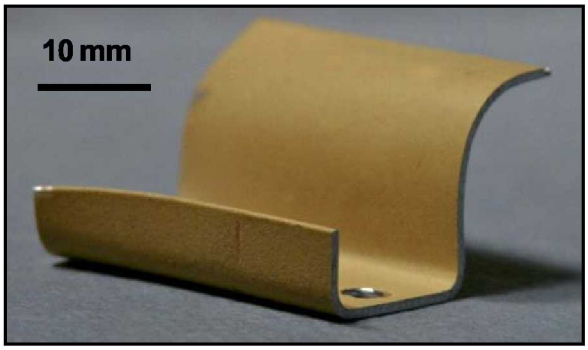

(b) Image of high-stiffness region cross section (A-A′).

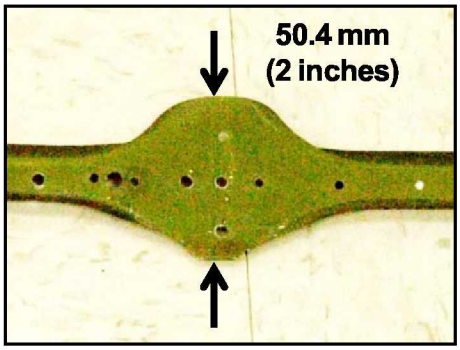

(c) Photograph of low-stiffness region.

Figure 2. Photographs of an MD 500 longeron.

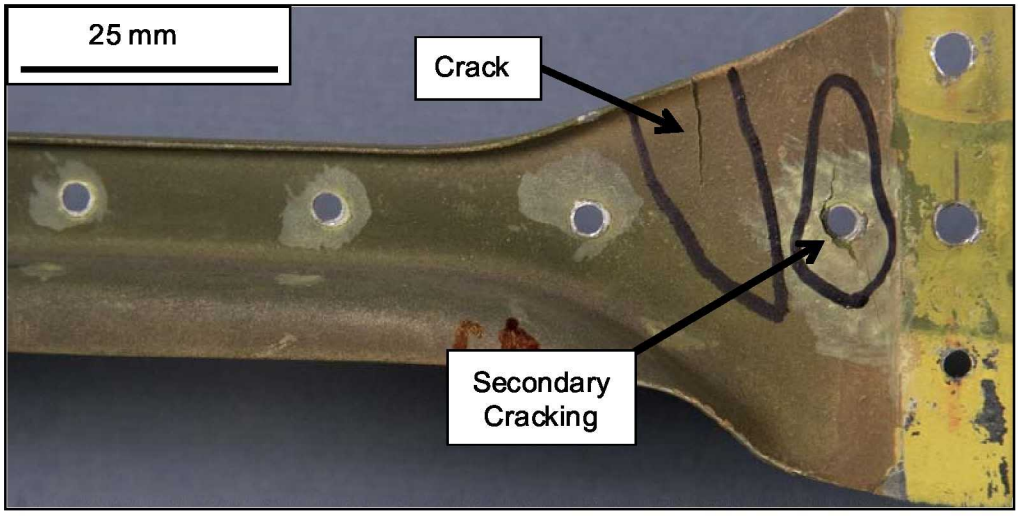

(a) Photograph of typical longeron crack with secondary cracking (Longeron #2, Crack #2).

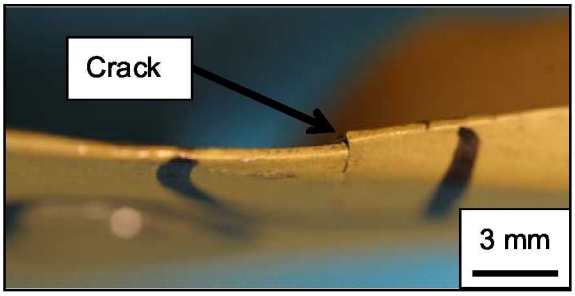

(b) Photograph of crack with residual shear displacment (Longeron #4, Crack #1).

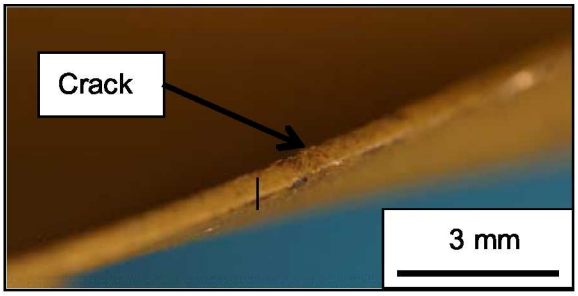

(c) Photograph of crack without residual shear displacment (Longeron #4, Crack #2).

Figure 3. Photographs of typical cracks found in MD 500 longerons.

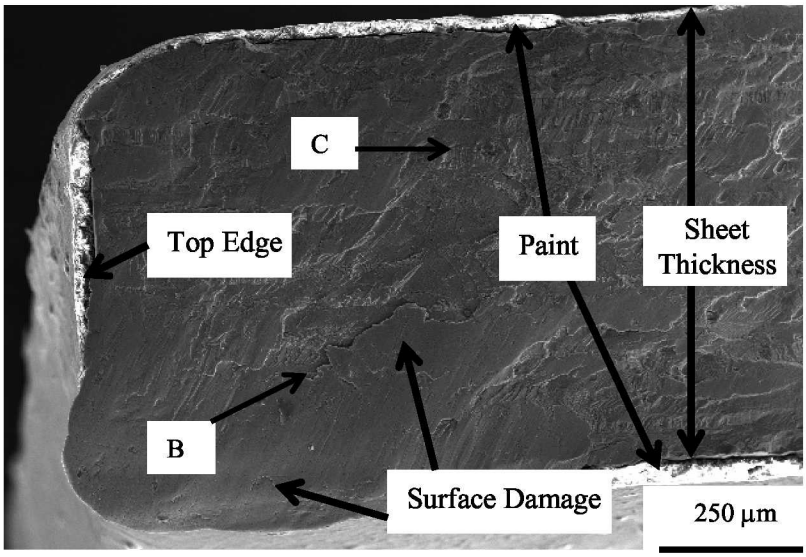

(a) Lower-magnification image showing the entire sheet thickness.

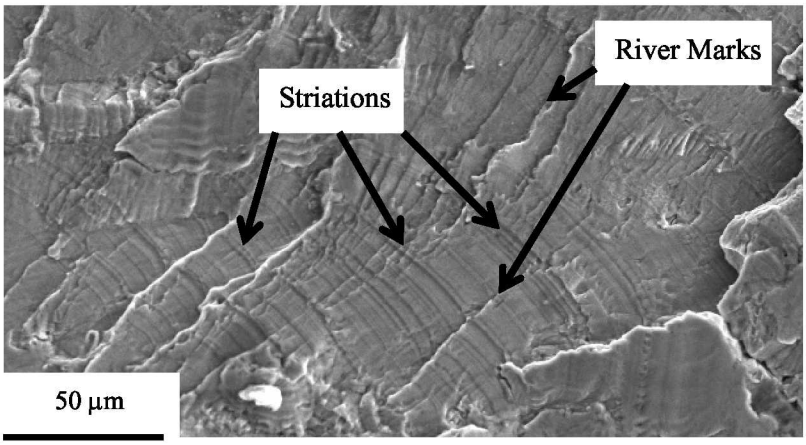

(b) Higher-magnification image of fatigue striations, region B.

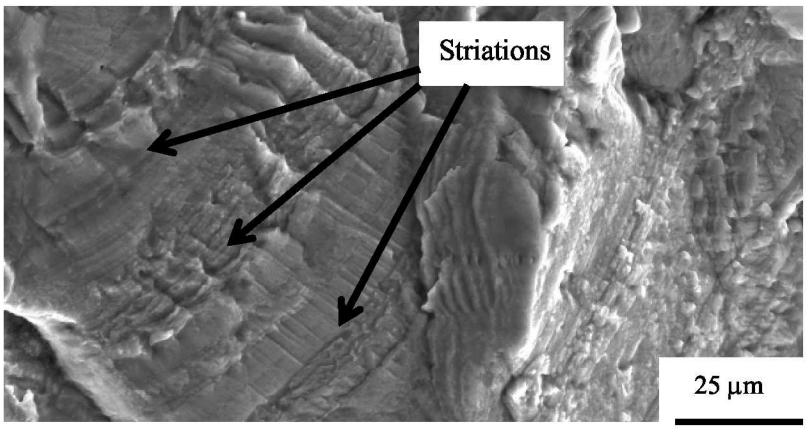

(c) Higher-magnification image of fatigue striations, region C.

Figure 4. SEM crack-surface micrographs for Longeron #1, Crack #1.

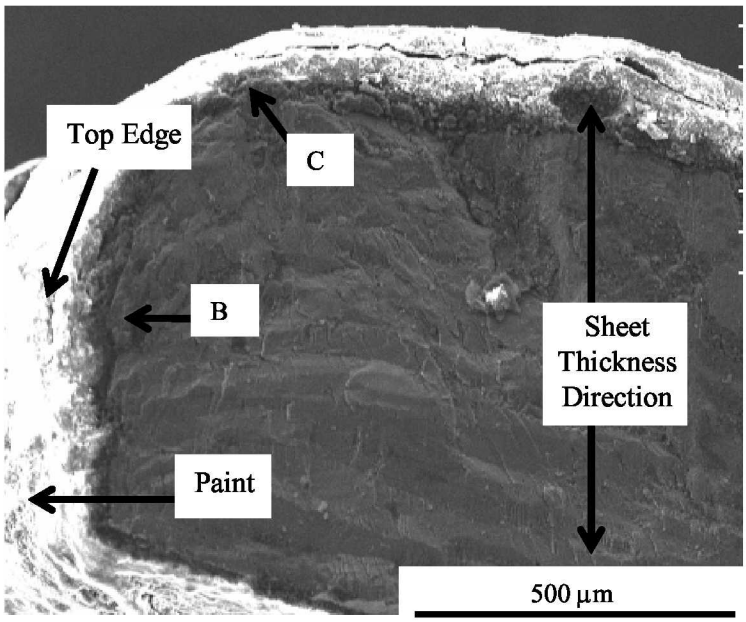

(a) Lower-magnification image showing the entire sheet thickness.

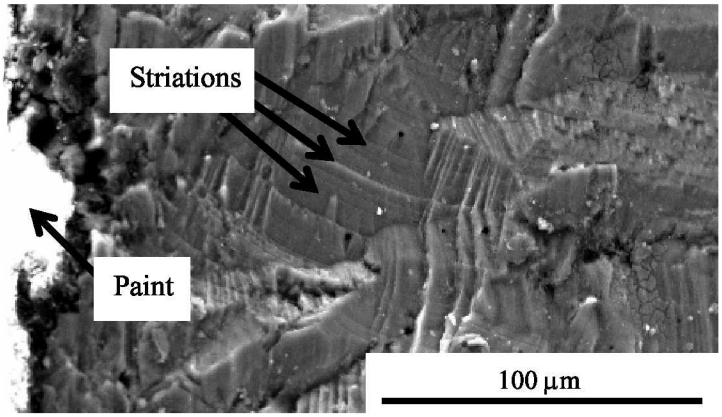

(b) Higher-magnification image of fatigue striations, region B.

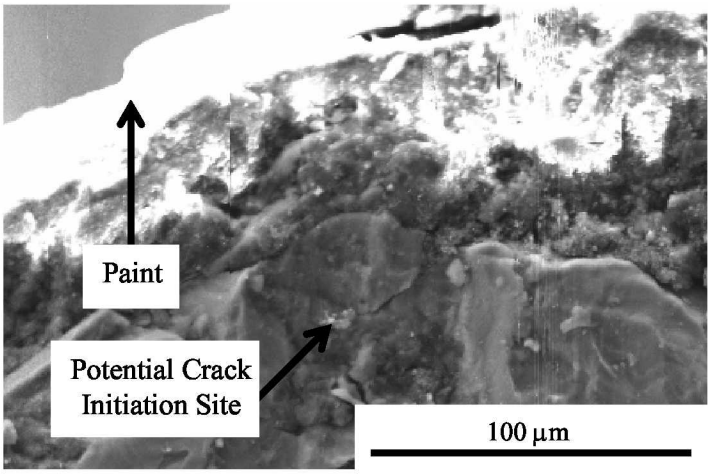

(c) Higher-magnification image of apparent crack initiation site, region C.

Figure 5. SEM crack-surface micrographs for Longeron #1, Crack #2.

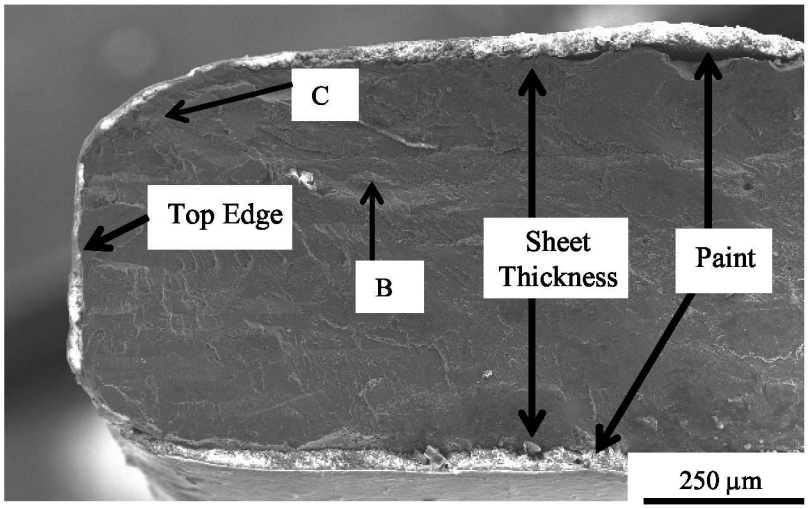

(a) Lower-magnification image showing the entire sheet thickness.

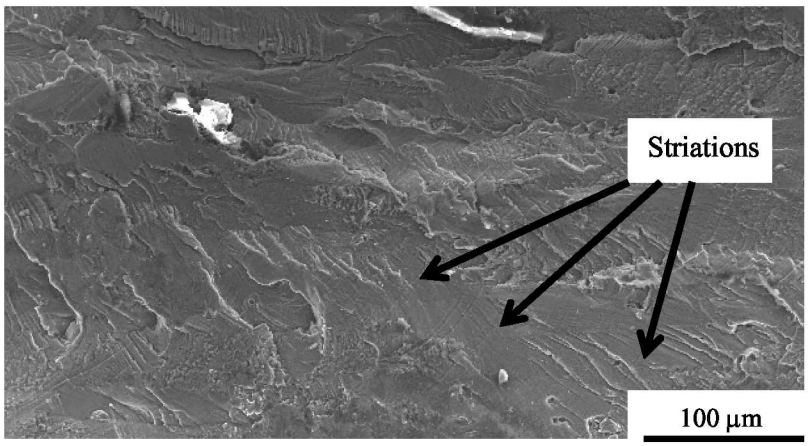

(b) Higher-magnification image of fatigue striations, region B.

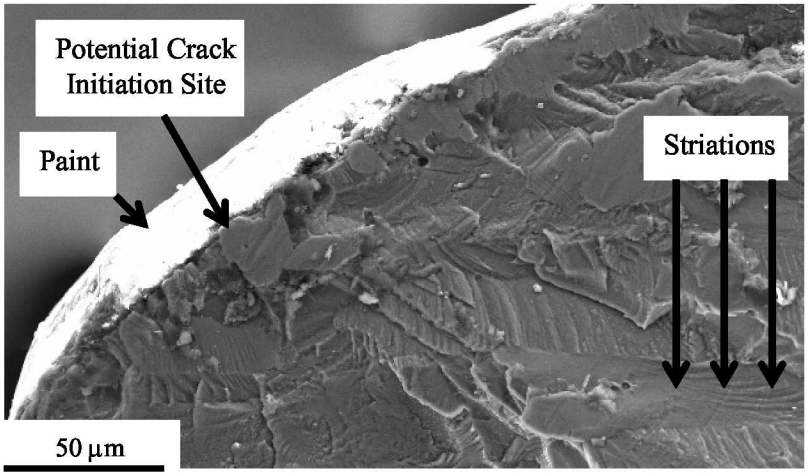

(c) Higher-magnification image of apparent crack initiation site, region C.

Figure 6. SEM crack-surface micrographs for Longeron #1, Crack #3.

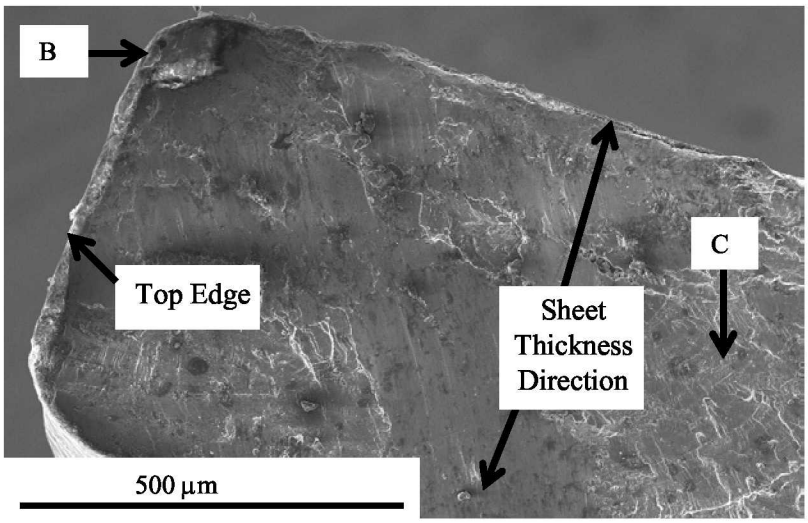

(a) Lower-magnification image showing the entire sheet thickness.

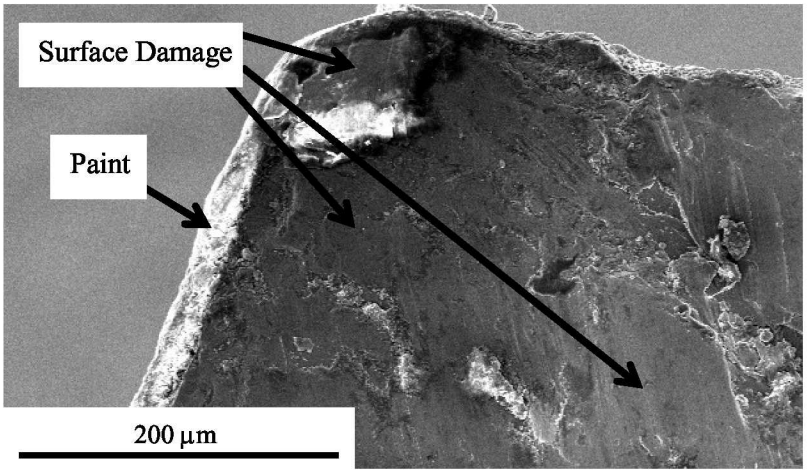

(b) Higher-magnification image of crack-surface damage, region B.

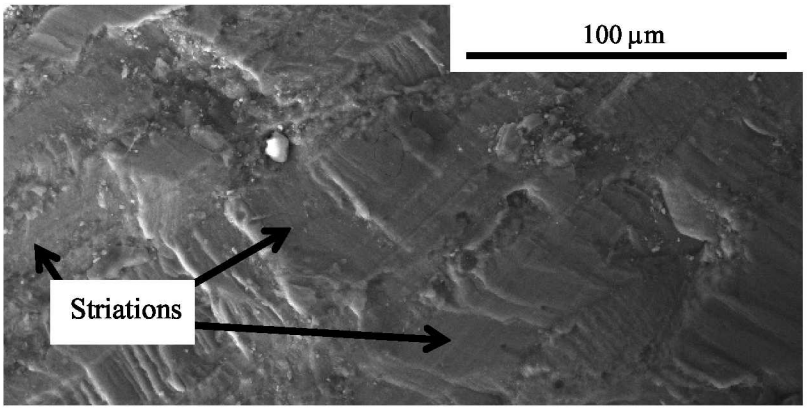

(c) Higher-magnification image of fatigue striations, region C.

Figure 7. SEM crack-surface micrographs for Longeron #2, Crack #1.

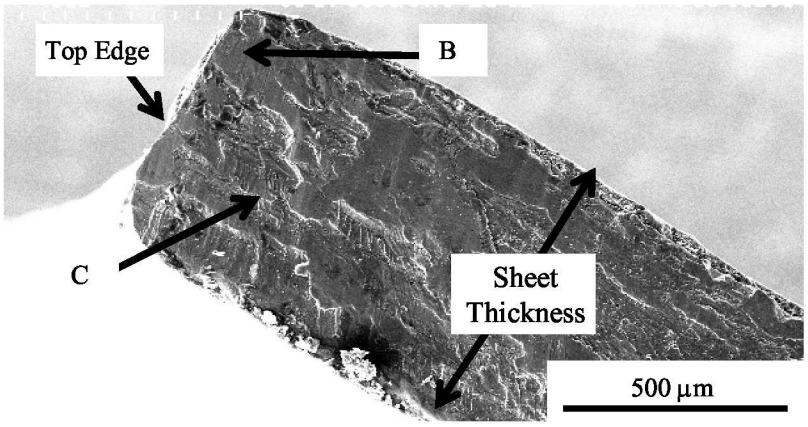

(a) Lower-magnification image showing the entire sheet thickness.

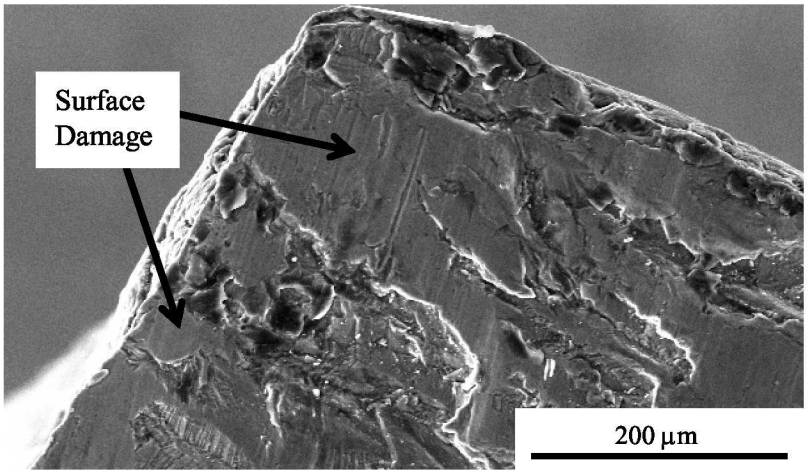

(b) Higher-magnification image surface damage, region B.

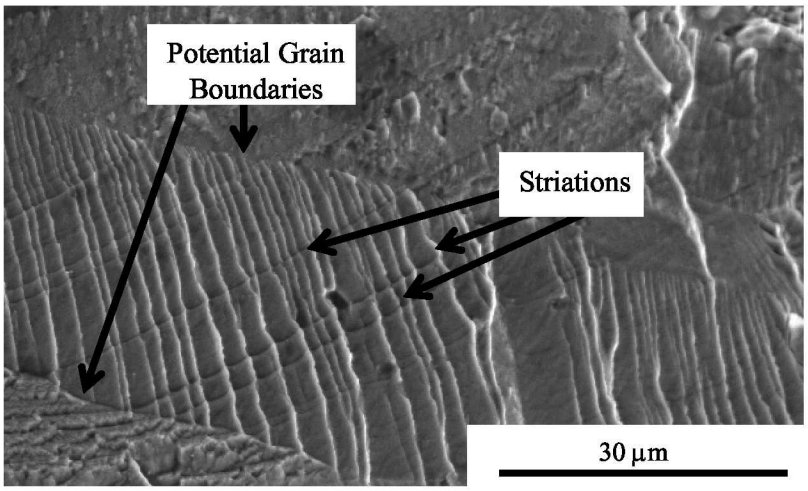

(c) Higher-magnification of fatigue crack striations, region C.

Figure 8. SEM crack-surface micrographs for Longeron #2, Crack #2.

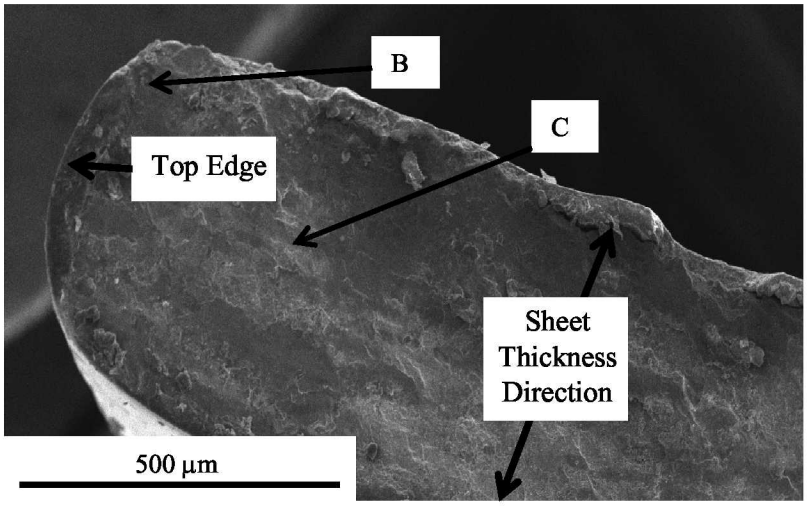

(a) Lower-magnification image showing entire sheet thickness.

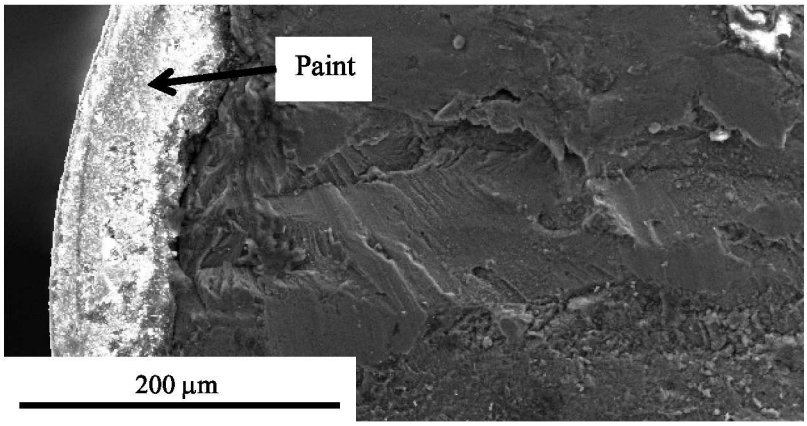

(b) Higher-magnification image of surface damage, region B.

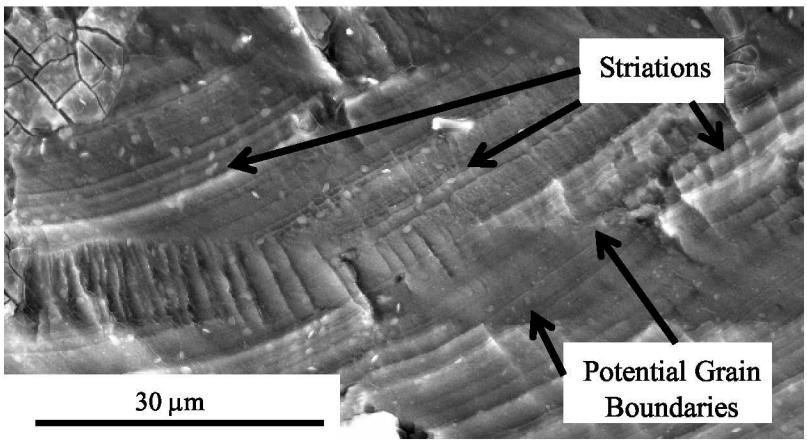

(c) Higher-magnification image of fatigue striations, region C.

Figure 9. SEM crack-surface micrographs for Longeron #3, Crack #1.

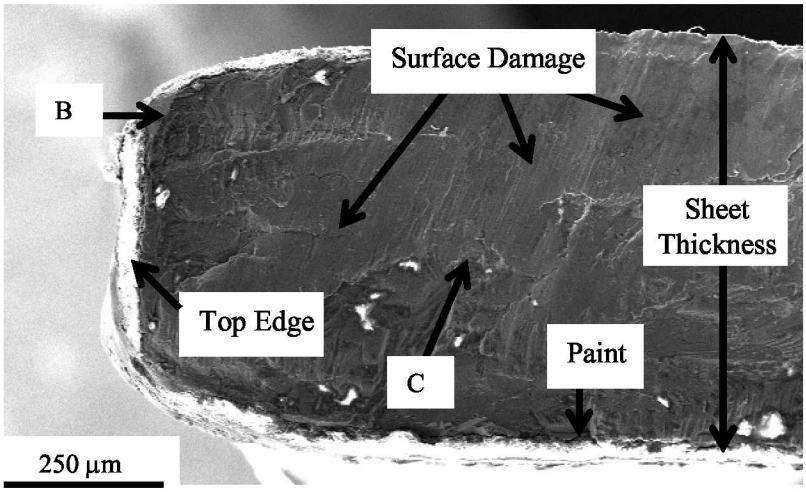

(a) Lower-magnification image showing the entire sheet thickness.

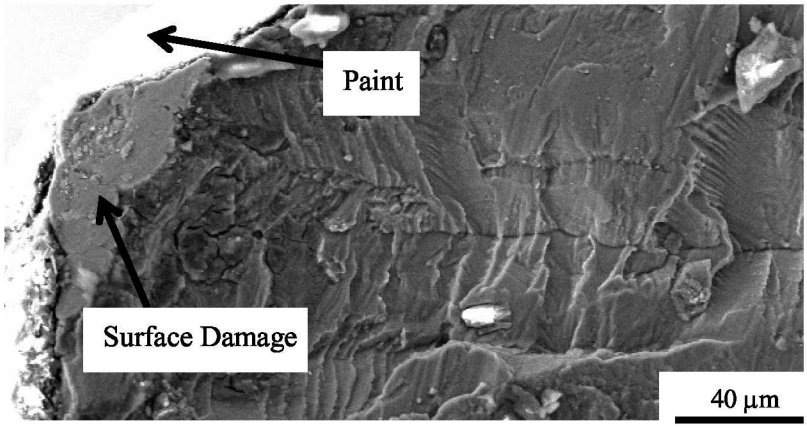

(b) Higher-magnification image of surface damage, region B.

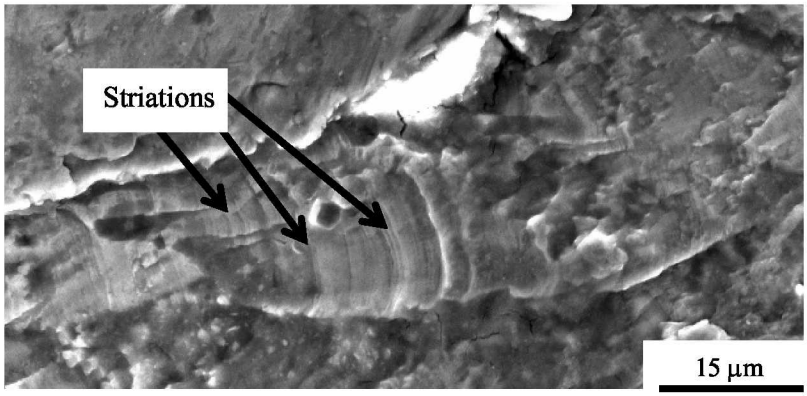

(c) Higher-magnification image of fatigue striations, region C.

Figure 10. SEM crack-surface micrographs for Longeron #4, Crack #1.

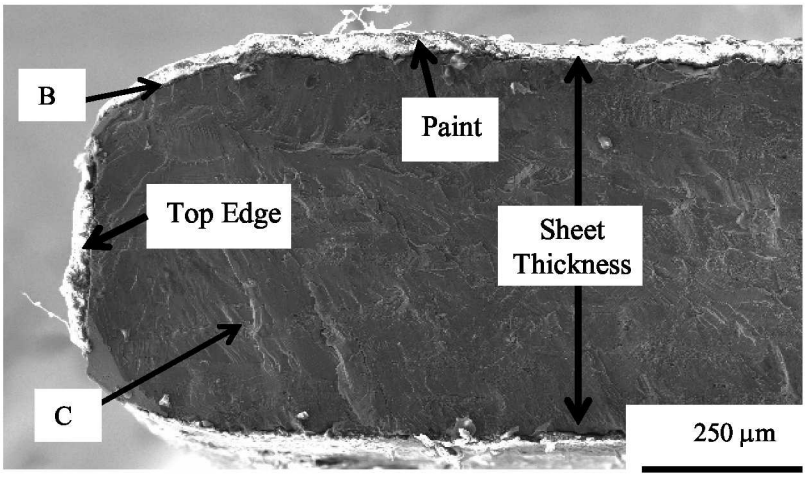

(a) Lower-magnification image showing the entire sheet thickness.

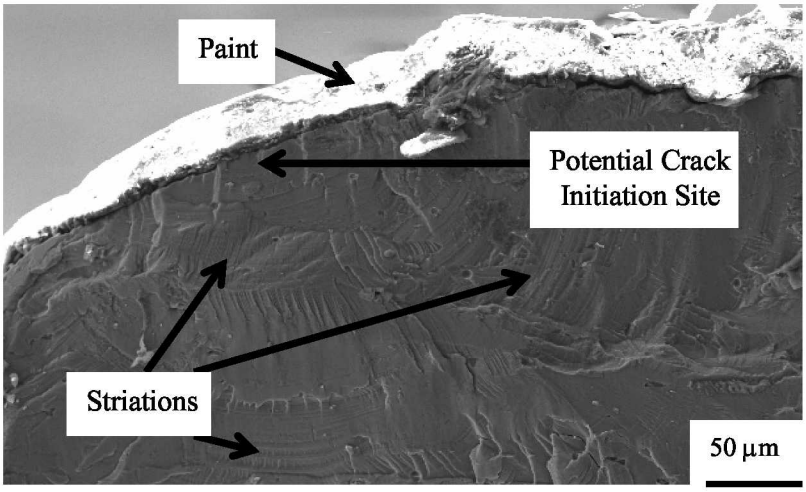

(b) Higher-magnification image of apparent crack initiation site, region B.

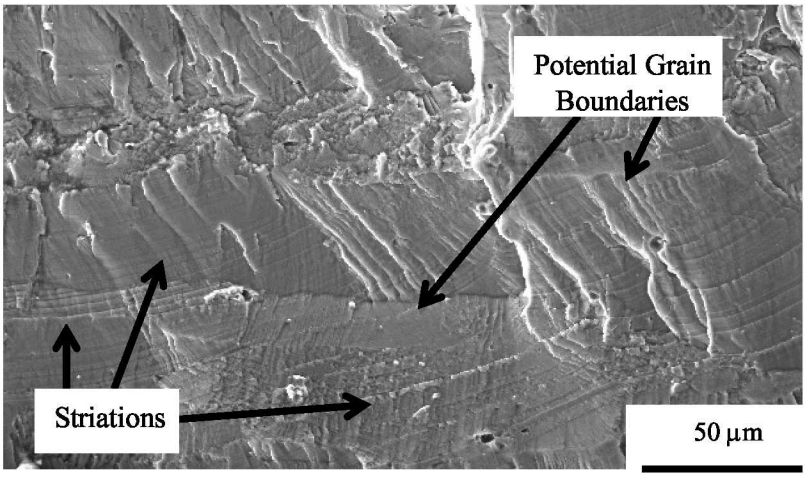

(c) Higher-magnification image of fatigue striations, region C.

Figure 11. SEM crack-surface micrographs for Longeron #4, Crack #2.

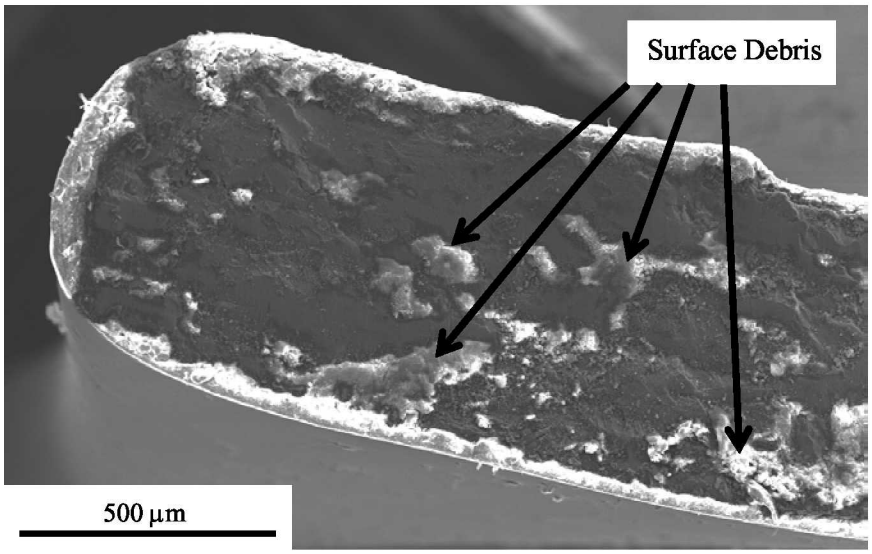

(a) Crack surface with debris before cleaning.

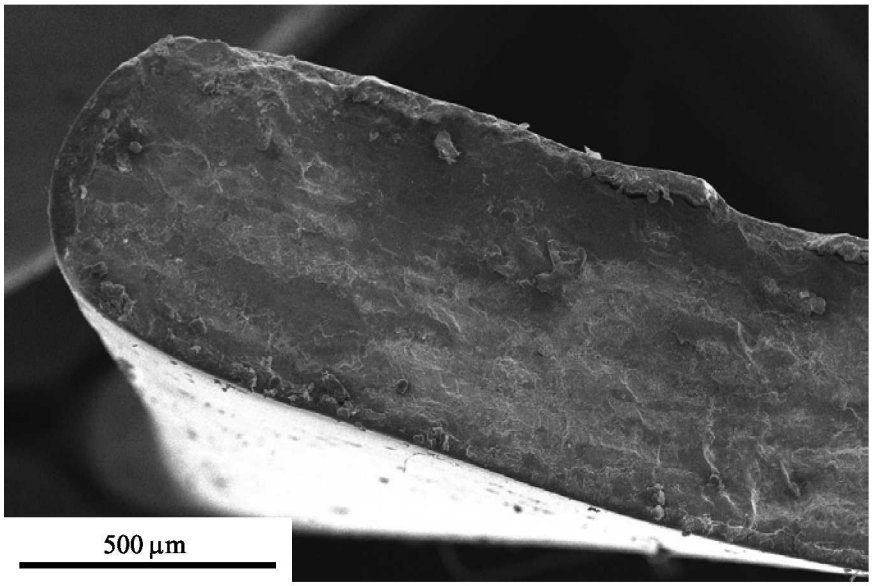

(b) Crack surface after cleaning.

Figure 12. Images of typical crack surface (Longeron #3, Crack #1).

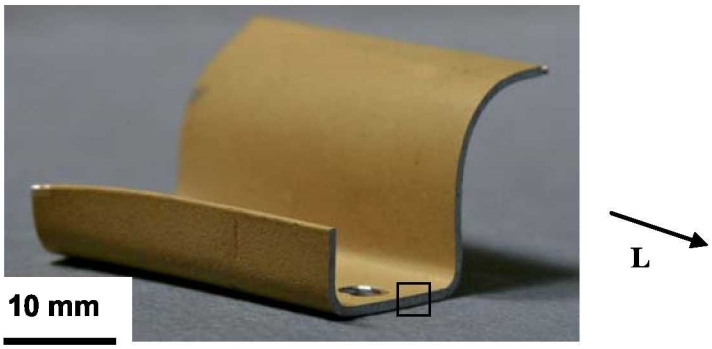

(a) Photograph of longeron cross section used for analysis.

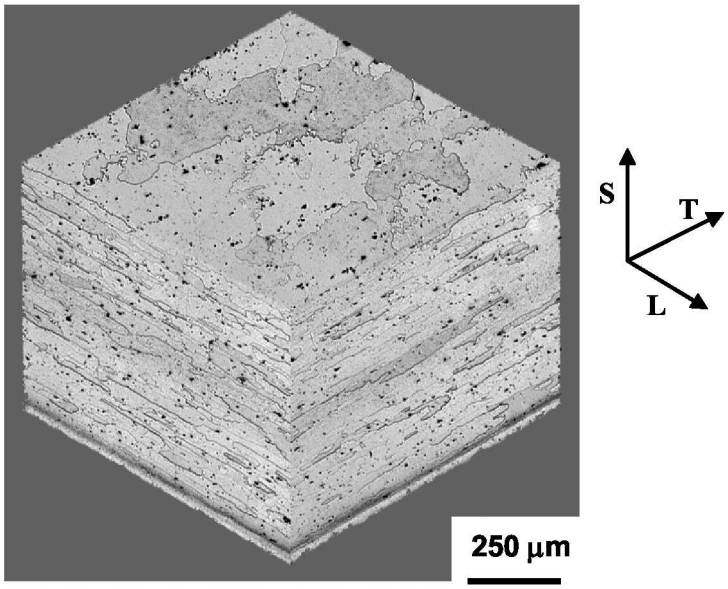

(b) Metallurgical images arranged as an orthogonal metallurgical cube.

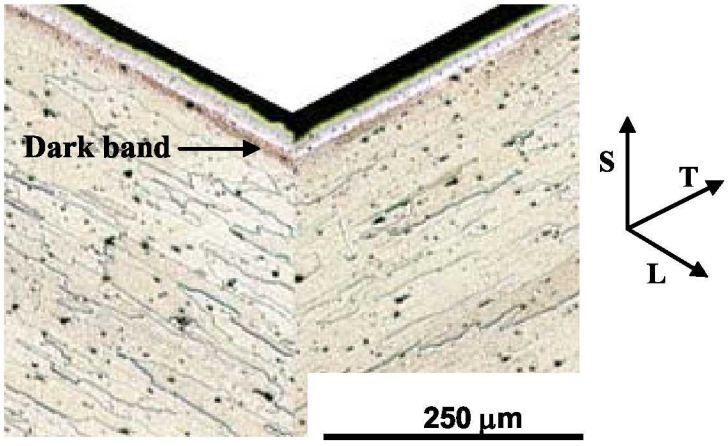

(c) High-magnification image of grain structure.

Figure 13. Results of metallurgical analysis of aluminum alloy 7075 longeron sheet material.

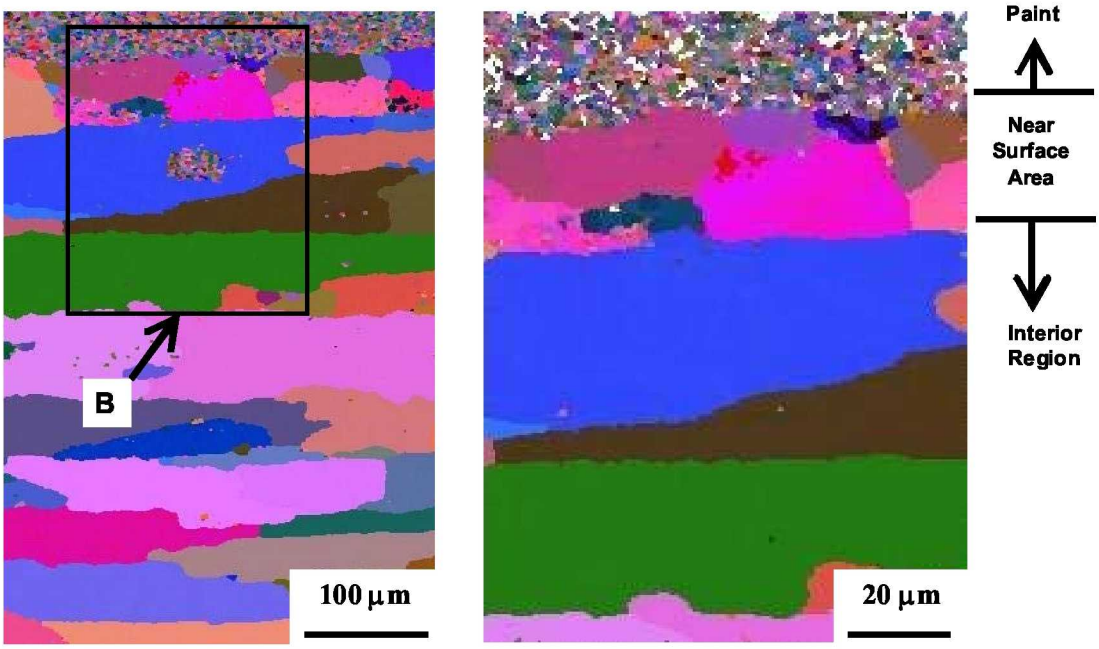

(a) EBSD crystal orientation map (b) Higher-magnification EBSD map, region B.

Figure 14. Near-surface crystal orientation maps generated by EBSD.

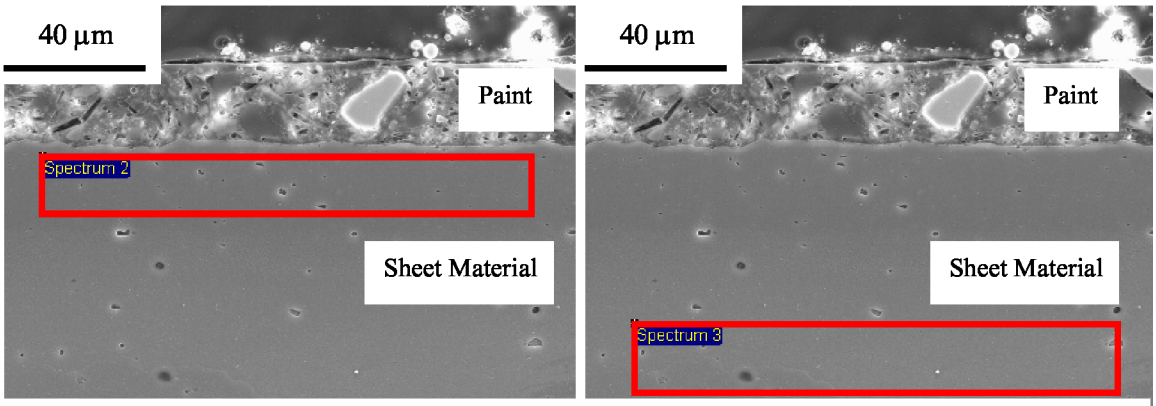

(a) Near-surface area analyzed (b) Interior area analyzed

Figure 15. Near-surface and interior regions used for chemical analysis.